

PIR: Remote Sensing Image-Text Retrieval with Prior Instruction Representation Learning

Jiancheng Pan¹, *Student Member, IEEE*, Muyuan Ma, Qing Ma², *Member, IEEE*,
 Cong Bai³, *Member, IEEE*, and Shengyong Chen⁴, *Senior Member, IEEE*,

Abstract—Remote sensing image-text retrieval constitutes a foundational aspect of remote sensing interpretation tasks, facilitating the alignment of vision and language representations. This paper introduces a prior instruction representation (PIR) learning paradigm that draws on prior knowledge to instruct adaptive learning of vision and text representations. Based on PIR, a domain-adapted remote sensing image-text retrieval framework PIR-ITR is designed to address semantic noise issues in vision-language understanding tasks. However, with massive additional data for pre-training the vision-language foundation model, remote sensing image-text retrieval is further developed into an open-domain retrieval task. Continuing with the above, we propose PIR-CLIP, a domain-specific CLIP-based framework for remote sensing image-text retrieval, to address semantic noise in remote sensing vision-language representations and further improve open-domain retrieval performance. In vision representation, we utilize the prior-guided knowledge of the remote sensing scene recognition by building a belief matrix to select key features for reducing the impact of semantic noise. In text representation, we use the previous time step to cyclically activate the current time step to enhance text representation capability. A cluster-wise Affiliation Loss (AL) is proposed to constrain the inter-classes and to reduce the semantic confusion zones in the common subspace. Comprehensive experiments demonstrate that PIR could enhance vision and text representations and outperform the state-of-the-art methods of closed-domain and open-domain retrieval on two benchmark datasets, RSICD and RSITMD.

Index Terms—Image-Text Retrieval; Prior Instruction Representation; Vision-Language Model; Remote Sensing

I. INTRODUCTION

REMOTE Sensing Image-Text Retrieval (RSITR) aims to use image patches (text) to search for matching text (image patches) from large-scale remote sensing databases collected by satellites or aerial drones to obtain valuable information. Due to its important applications [1] in natural resource exploration and disaster monitoring [2], RSITR has received much attention from researchers. In recent years, the rapid expansion of remote sensing data [3] coupled with

Jiancheng Pan (e-mail: jiancheng.pan.plus@gmail.com) and Muyuan Ma (e-mail: mamy22@mails.tsinghua.edu.cn) are with the Ministry of Education Key Laboratory for Earth System Modeling, and Department of Earth System Science, Tsinghua University, Beijing, 10084, China. Cong Bai (e-mail: congbai@zjut.edu.cn) is with the College of Computer Science and Technology, Zhejiang University of Technology, Hangzhou 310023, China. (Corresponding Author: Cong Bai.) Qing Ma (e-mail: maqing@zjut.edu.cn) is with the College of Science, Zhejiang University of Technology, Hangzhou 310023, China. Shengyong Chen (e-mail: sy@ieec.org) is with the School of Computer Science and Engineering, Tianjin University of Technology, Tianjin 300384, China.

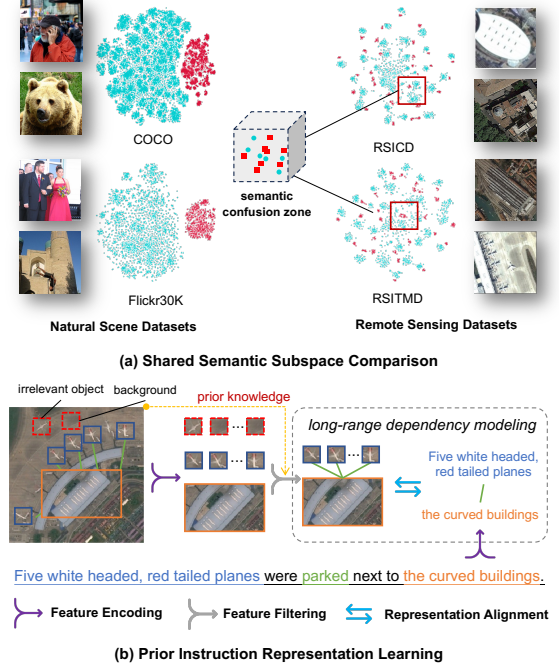


Fig. 1. (a): Shared semantic subspace comparison in natural scene and remote sensing datasets, the red squares represent vision embeddings, and the blue circles represent text embeddings; (b): Pipeline of our proposed PIR to reduce the influence of semantic noise.

advancements in cross-modal retrieval techniques [4] has provided substantial data and technical support for RSITR.

According to different training paradigms, RSITR can be divided into closed and open-domain retrieval. Closed-domain retrieval is a supervised training and retrieval under a single dataset, but it is less capable of retrieving more complex ground elements. In closed-domain retrieval, most existing methods are CNN-based [5] vision representation and RNN-based [6] text representation using pair-wise triplet loss [7] for optimization. Abdullah et al. [8] first applied modality fusion to solve the remote sensing image-text matching problem. Lv et al. [9] used knowledge distillation to transform the fusion information of modality to vision and text representation learning. Mi et al. [10] utilized a knowledge graph to enrich text semantics and to reduce the information gap between vision and language. Yuan et al. [11] developed an RSCTIR model to understand multi-level visual semantics based on global and local information. Pan et al. [12] proposed a

scene-aware aggregation network to improve the fine-grained perception of the scene. These approaches benefit from a good vision and text representation and perform poorly for long-range dependency modelling [13], [14]. Open-domain retrieval is fine-tuned on a small dataset after pre-training on an additional large-scale dataset with better ground element recognition. CLIP [15] inspired efforts with powerful zero-shot learning on visual interpretation tasks in open-domain retrieval. Subsequently, RemoteCLIP [16], GeoRSCLIP [17], and SkyCLIP [18] models were introduced to establish a foundation vision-language model for remote sensing (RSVLM) and improve large-scale open-domain image-text retrieval performance. Their objective is to establish a foundation RSVLM rather than delving into methods to enhance the visual representation of remote sensing.

Figure 1(a) visualizes the subspaces on the natural scene datasets COCO [19] and Flickr30K [20], and remote sensing datasets RSICD [3] and RSITMD [21] using t-SNE [22]. In the natural scene subspace, image and text representations are separated more significantly than in the remote sensing subspace. Unlike natural images, small-scale objects in remote sensing images are more prone to the interference of semantic noise [11], such as background, irrelevant objects, etc. Excessive attention to semantic noise biases the vision and text representations and causes semantic confusion zones [12] (vision embeddings and text embeddings crossover zones), which greatly affects retrieval performance. Yuan et al. [21] used a redundant feature filtering network to filter useless features. Pan et al. [12] proposed a scene-aware aggregation network to reduce the semantic confusion zones in the common subspace. Nevertheless, these methods are based on CNN-based vision representation and RNN-based text representation, which is not effective for long-range dependency modeling [23] and the growth of remote sensing data. With the powerful performance of Transformer in computer vision [24] and natural language processing [25], Transformer-based vision and text representations enable retrieval performance to be further improved. Zhang et al. [26] designed a decoupling module based on Transformer to obtain invariant features in the modalities. However, this method ignores the remote sensing data characteristics [11], [12], making limited improvement in retrieval performance. In short, a framework specific to remote sensing data becomes necessary.

We propose a **P**rior **I**nstruction **R**epresentation (PIR) to reduce the influence of semantic noise as shown in Figure 1(b). Firstly, PIR-ITR is designed to utilize prior knowledge of remote sensing scene recognition [27] to perform long-range dependency modelling, ensuring the unbiased vision and text representations, as shown in Figure 2. Two progressive attention encoder (PAE) structures, Spatial-PAE and Temporal-PAE, are proposed to perform long-range dependency modelling to enhance key feature representation. Spatial-PAE utilizes external knowledge to enhance visual-spatial perception. Temporal-PAE is applied to reduce the inaccuracy of position information by leveraging the previous time step to activate the current time step cyclically. In vision representation, we filter features by building a belief matrix, aiming for an unbiased vision representation. In text representation, we de-

sign Temporal-PAE to obtain an unbiased text representation. For the inter-class similarity [21] in the remote sensing data domain, a cluster-wise attribution loss is proposed to constrain the inter-classes and reduce the semantic confusion zones in the common subspace. Extensive experiments are conducted on two benchmark datasets, RSICD [3], and RSITMD [21], to demonstrate the effectiveness of our approach, resulting in improvements of 4.9% and 4.0% on the RSICD and RSITMD respectively. Based on the PIR, we propose a two-stage CLIP-based method, PIR-CLIP, to address semantic noise in remote sensing vision-language representations and improve open-domain image-text retrieval further. Unlike vanilla CLIP structure, visual prior knowledge is used to instruct visual representations, as shown in Figure 2. It has a universal model architecture and higher retrieval performance than PIR-ITR, which adjusts the visual representation through instruction embeddings and only needs to fine-tune a few parameters, with 7.3% and 9.4% improvement over open-domain state-of-the-art methods on RSICD dataset and RSITMD dataset, respectively.

Our key contributions are as follows:

- We propose a prior instruction representation (PIR) learning paradigm, which utilizes prior knowledge of the remote sensing scene recognition for unbiased representation to enhance vision-language understanding, which can be applied to closed-domain and open-domain retrieval.
- PIR-ITR is proposed for closed-domain retrieval. Two PAE structures, Spatial-PAE and Temporal-PAE, are proposed to perform long-range dependency modelling to enhance key feature representation. we use instruction embedding to filter features by building a belief matrix aiming for an unbiased vision representation. Temporal-PAE improves text representation by using the previous time step to activate the current time step.
- PIR-CLIP, a two-stage CLIP-based method with prior instruction representation learning, is proposed to address semantic noise in remote sensing vision-language representations and improve open-domain retrieval performance further. First, the image and text encoders are pre-trained on five million coarse-grained remote sensing image-text pairs, and then vision instruction fine-tuning is performed on fine-grained remote sensing image-text pairs.
- A cluster-wise attribution loss is proposed to constrain the inter-classes and reduce the semantic confusion zones in the common subspace.

Compared with our previous work [28], we further extend the PIR learning paradigm to open-domain retrieval based on the former closed-domain retrieval. This work designs PIR-ITR with a soft belief strategy to tune visual representation dynamically and proposes PIR-CLIP based on PIR, which address semantic noise in remote sensing vision-language representations and further improves the remote sensing image-text retrieval performance, especially in open-domain retrieval performance, as well as adds more detailed experiments to validate the effectiveness of our method.

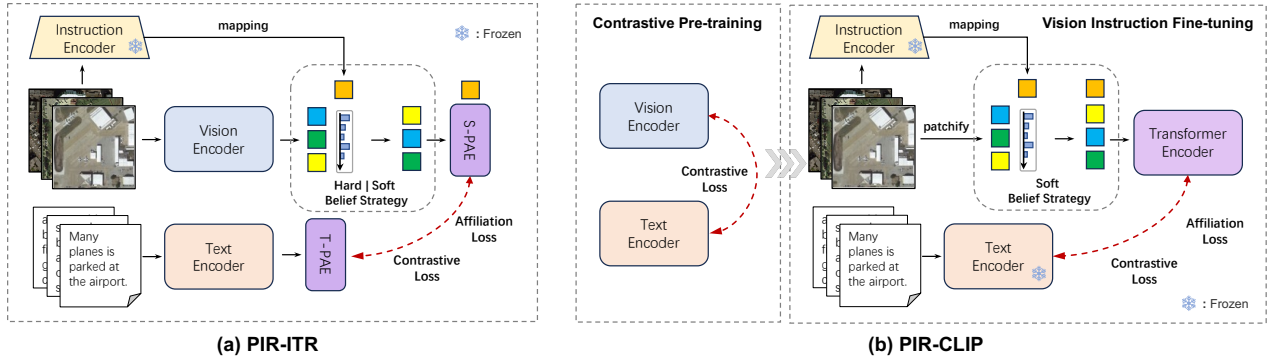


Fig. 2. Image-Text Alignment with PIR Learning. (a) PIR-ITR framework with Spatial-PAE (S-PAE) and Temporal-PAE (T-PAE) for unbiased representation in the common subspace; (b) PIR-CLIP framework, a two-stage strategy to pre-train vision and text encoders on large-scale remote sensing image-text pairs, then perform vision instruction fine-tuning for open-domain retrieval, which adjusts the visual representation through instruction embeddings and only needs to fine-tune a few parameters.

II. RELATED WORK

A. Remote Sensing Image-text Retrieval

Closed-domain method is a supervised method for training and retrieval under a single dataset, but it is less capable of retrieving more complex ground elements. Some works [8], [10], [11], [26], [29] only perform self-interaction on the same modality to obtain an enhanced modal semantic representation. [8], [29] used the information of different modalities to obtain a joint semantic representation. Might et al. [10] proposed a knowledge-based method to solve the problem of coarse-grained textual descriptions. Yuan et al. [11] proposed a network structure based on global and local information, using attention-based modules to fuse multi-level information dynamically. Zhang et al. [26] designed a reconstruction module to reconstruct the decoupled features, which ensures the maximum retention of information in the features. Some others [9], [21], [30], [31] use information between different attention mechanisms or shared parameter networks for interactive learning. Lv et al. [9] propose a fusion-based association learning model to fuse image and text information across modalities to improve the semantic relevance of different modalities. Particularly, Yuan et al. [30] used a shared pattern transfer module to realize the interaction between modalities, solving the semantic heterogeneity problem between different modal data. Cheng et al. [31] propose a semantic alignment module that uses an attention mechanism to enhance the correspondence between image and text. Yuan et al. [21] suggest an asymmetric multimodal feature matching network to adapt multiscale feature inputs while using visual features to guide text representation. These methods are based on partial simulations of the real complex remote sensing world and fail to learn fine-grained perceptions of the environment.

Open-domain method is fine-tuned on a small dataset after pre-training on an additional large-scale dataset, with better ground element recognition. Since the advent of CLIP [15], CLIPs for tasks in the remote sensing [16]–[18], [32] have emerged. Some work [32] has begun early exploration of fine-tuning CLIP to enhance remote sensing image-text retrieval, but only got poor performance. Further, Chen et al.

[16] proposed RemoteCLIP, the first vision-language model for remote sensing, to implement language-guided retrieval and zero-shot tasks. Zhang et al. [17] published RS5M, a large-scale remote sensing image-text dataset with more than 5 million images, and utilized geographic information to train the vision-language model GeoRSClip. Coincidentally, a new remote sensing benchmark dataset, SkyScript, and a benchmark model, SkyCLIP, were proposed by Wang [18] et al. However, their goal is mainly to build a foundation vision-language model for remote sensing (RSVLM) without further exploring how to enhance the visual representation of remote sensing. We aim to propose a CLIP-based model that can upgrade the performance of remote sensing large-scale open-domain retrieval based on foundation RSVLM.

B. Cross-Attention Mechanism

Different from self-attention [33], cross-attention is an attention mechanism in Transformer architecture that mixes two different embedding sequences. These two different embedding sequences come from different modalities or different outputs. Cross-attention [34] is widely used in various deep learning tasks, including image-text retrieval tasks [35], [36].

Lee et al. [35] introduced an innovative *Stacked Cross Attention* approach that allows for contextual attention from images and sentences. Wei et al. [37] presented the *Multi-Modality Cross Attention Network* for aligning images and sentences, capturing relationships within and across modalities in a single deep model. CASC framework [38] combines cross-modal attention for local alignment with multilabel prediction for global semantic consistency. However, these methods are customized and cannot be used directly elsewhere. Diao et al. [36] develop two plug-and-play regulators to automatically contextualize and aggregate cross-modal representations. The above methods forget to increase network depth for large amounts of time-scale and spatial-scale data. Therefore, a universal and easily adjustable cross-attention structure should be more desired.

III. REMOTE SENSING IMAGE-TEXT RETRIEVAL

We summarise the current remote sensing image-text retrieval (RSITR) methods, first defining a generic image and

text encoding scheme and then deforming the presentation of the various available image-text alignment schemes.

A. Generic Image and Text Encoding

One route to interpreting remote sensing images is aligning images and text at the semantic level. Remote sensing image-text retrieval is the foundation task for this alignment, mainly encoding image and text features through visual and text encoders and then achieving alignment of image and text in the common semantic space. Among RSITR methods, CNN-based image encoder [8]–[11], [21], [30], [31], [39] and Transformer-based image encoder [40], [41] are used to image features. Given a RGB-formatted image $I_{img} \in \mathbb{R}^{3 \times H \times W}$, it is common practice to encode by a image encoder E_{img} to get a global correlated feature $F_{cls} \in \mathbb{R}^{d \times 1}$ ([CLS]) and local correlated features $F_v \in \mathbb{R}^{d \times m}$ as

$$[f_{cls}, F_v] = E_{img}(I_{img}; \emptyset_{img}), \quad (1)$$

where \emptyset_{img} is the fine-tuning weights, $[\cdot, \cdot]$ indicates stacking and concatenation on the sequence length dimension. If the image encoder is CNN-based, f_{cls} is the high-level features, and F_v is the lower-level feature ensemble. In RSITR methods, the RNN-based feature extraction approach [8], [11], [21] and the Transformer-based text feature extraction approach [10], [26] are primary. Compared to RNN [42], Transformer [33] considers all positions in the input sequence simultaneously, thus capturing global semantic relationships and long-range dependencies. Given a text T_{txt} , it is common practice to get the global correlated feature $t_{cls} \in \mathbb{R}^{d \times 1}$ ([CLS]) and local correlated features $E_t \in \mathbb{R}^{d \times n}$ as

$$[t_{cls}, F_t] = E_{txt}(T_{txt}; \emptyset_{txt}), \quad (2)$$

where $E_{txt}(\cdot)$ denotes the text encoder, \emptyset_{txt} is the fine-tuning weights and n is the number of local correlated features. For RNN-based text encoders, t_{cls} generally comes from pooled averaging of F_t . Specific methods vary for $[f_{cls}, F_v]$ and $[t_{cls}, F_t]$ extraction.

B. Various Image-Text Alignment

A simple way to achieve this alignment is by fine-tuning the parameters of vision and text encoders with learnable weights \emptyset_{img} and \emptyset_{txt} , aligning f_{cls} and t_{cls} globally, such as the VSE [43]. This method performs better on datasets with a higher proportion of image-text pairs, such as COCO [19], but its improvement is limited in remote sensing applications. Methods such as SCAN [39], CAMP [35] and CAM-ERA [44] represent images or texts more comprehensively by introducing visual and textual feature-level interactions $E_{img-txt}(F_v, F_t; \emptyset_{img-txt})$. These methods do not seem to be able to directly and significantly enhance the remote sensing imagery for representation, as the remote sensing scale is variable, and fine-grained alignment is not easy to achieve. In most RSITR methods, the visual information is expanded from various latitudes because the remote sensing imagery contains many redundant information. AMFMN [21] and SWAN [12] perform multi-scale feature fusion of f_{cls} and F_v and extracts salient features of remote sensing images by redundant feature filtering. GaLR [11] incorporates F_v and external object-level knowledge F_l processed by graph

convolutional networks (GCN), with feature-level interactions $E_{img-img}(F_v, F_l; \emptyset_{img-img})$. These methods are aligned to optimised visual and textual features.

IV. PRIOR INSTRUCTION REPRESENTATION LEARNING

We first define prior instruction representation (PIR) learning in RSITR and then provide a detailed description of PIR-ITR, CLIP-baed PIR-CLIP.

A. Preliminaries

There are much semantic noise in remote sensing images, which bias the representation of visual semantics. Some methods [45]–[50] introduce some additional prompts or instructions to guide the models for better representations. Taking inspiration from these methods, we use ResNet [51] pre-trained on AID dataset [52] as an instruction encoder $E_{inst}(I_{img}; \emptyset_{ins})$, where \emptyset_{ins} is the pre-trained weights, to obtain instruction embeddings $\in \mathbb{R}^{d \times 1}$. As mentioned above GaLR [11] incorporates F_v and external object-level knowledge processed by GCN, but its role as an element of feature fusion may influence the intrinsic representations of the image. Different from GaLR, instruction embeddings serve as instructions to help visual feature representation. We can express this as a pseudo-formula as $E_{img-img}([f_{cls}, F_v]; f_{ins}, \emptyset_{img-img})$. Our goal is to filter out unbiased visual features from $[f_{cls}, F_v]$ with the help of f_{ins} .

B. Belief Strategy

Unlike natural images, small-scale objects in remote sensing images are more susceptible to semantic noise from background or irrelevant objects, significantly impacting visual representation. The belief strategy addresses this by first constructing a belief matrix using instruction embeddings, and then filtering features to achieve an unbiased visual representation, as shown in Figure 2.

The prior knowledge of remote sensing scene recognition f_{ins} is used to calculate the belief matrix $\mathcal{M}^{bel} \in \mathbb{R}^{1 \times (m+1)}$ on the local correlated features $[f_{cls}, F_v]$, and then sort and filter features with a hard belief strategy [28] as

$$\mathcal{M}^{bel} = \text{Softmax}(f_{ins}^T [f_{cls}, F_v]), \quad (3)$$

$$[f_{cls}, F_v] \xrightarrow[\text{Sort \& Filter}]{\mathcal{M}^{bel}} F'_v = [F_{:,r_1}, \dots, F_{:,r_k}], (r_k < m+1) \quad (4)$$

where $A \xrightarrow[\text{Sort \& Filter}]{\mathcal{M}^{bel}} B$ represents sort and filter the A sequence according to \mathcal{M}^{bel} to get the B sequence.

Despite the fact that the above strategy in practice, an empirical setting of the appropriate number of features r_k is required. To allow dynamic filtering of features, we propose a soft belief strategy without r_k . For batch ranking, the rank R_j of element $\mathcal{M}^{bel} \in \mathbb{R}^{1 \times (m+1)}$.

$$R_j = 1 + \sum_{k=1}^{m+1} \mathbb{I}(\mathcal{M}_k^{bel} < \mathcal{M}_j^{bel}), \quad (5)$$

where $\mathbb{I}(\cdot)$ is the indicator function to get the ranking weight of belief matrix scores, which is 1 when the condition inside the parenthesis is true, and 0 otherwise. For each element $F_{l,:} \in$

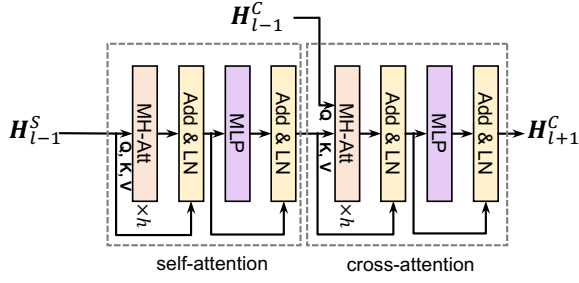


Fig. 3. Progressive Attention Encoder Layer.

$\mathbb{R}^{d \times 1}$ of dimension d in $[\mathbf{f}_{cls}, \mathbf{F}_v] \in \mathbb{R}^{d \times (m+1)}$, we get rank-weighted visual features as

$$\mathbf{F}'_v = \sum_{l=1}^{m+1} \mathbf{F}_{l,:} \left(\mathcal{M}_j^{\text{bel}} + \frac{1}{\sqrt{\mathbf{R}_j}} \right), \quad (6)$$

where $\mathbf{F}'_v = [\mathbf{f}_{r_1}, \mathbf{f}_{r_2}, \dots, \mathbf{f}_{r_k}]$, ($r_k = m + 1$). The new features are score-based and ranking-based i.e. relative ranked weighted features. This strategy is an alternative to Equation 4 does not require setting the number of visual features. This strategy makes the retrieval faster and better as shown in Table I. We also use this same strategy in PIR-CLIP to learn unbiased visual representation from large-scale data training.

C. Image-Text Alignment with PIR Learning

1) *Progressive Attention Encoder Layer*: Transformer Encoder Layer (TEL), a crucial element of the Transformer architecture, is integral to natural language processing and computer vision tasks. We design a Progressive Attention Encoder Layer (PAEL) based on TEL, which incorporates self-attention [33] and cross-attention [53], as shown in Figure 3. Different from self-attention, cross-attention merges two sequences regardless of modality. Given two different sequences $\mathbf{H}_{l-1}^S \in \mathbb{R}^{d \times N}$ and $\mathbf{H}_{l-1}^C \in \mathbb{R}^{d \times N}$, the calculation of PAEL (see Figure 3) can be expressed as

$$\mathbf{H}_l^S = \mathbf{H}_{l-1}^S + \text{LN}(\text{MHA}(\mathbf{H}_{l-1}^S, \mathbf{H}_{l-1}^S, \mathbf{H}_{l-1}^S)), \quad (7)$$

$$\mathbf{H}_{l+1}^S = \mathbf{H}_l^S + \text{LN}(\text{MLP}(\mathbf{H}_l^S)), \quad (8)$$

$$\mathbf{H}_l^C = \mathbf{H}_{l-1}^C + \text{LN}(\text{MHA}(\mathbf{H}_{l-1}^C, \mathbf{H}_{l+1}^S, \mathbf{H}_{l+1}^S)), \quad (9)$$

$$\mathbf{H}_{l+1}^C = \mathbf{H}_l^C + \text{LN}(\text{MLP}(\mathbf{H}_l^C)). \quad (10)$$

where $\text{MHA}(\cdot)$ is multi-head attention, $\text{LN}(\cdot)$ is the layer normalization, $\text{MLP}(\cdot)$ stands for multilayer perceptron, a common feedforward network. For the purpose of description, we can define the PAEL calculation as $\text{PAEL}(\mathbf{H}_{l-1}^S, \mathbf{H}_{l-1}^C)$.

2) *Progressive Attention Encoder*: We developed two distinct message transfer methods between PAELs: Spatial-PAE (S-PAE) and Temporal-PAE (T-PAE), to capture key feature representation, as illustrated in Figure 4.

Spatial-PAE (see Figure 4(a)) establishes a spatial connection to the input sequence from an external source using linear projection. Unlike fusion-based approaches [11], [12], [54], this connection relies on cross-attention. In long-range dependency modeling with PAELs, the self-attention mechanism has limited capacity to capture global information and requires extended sequence distances to form connections.

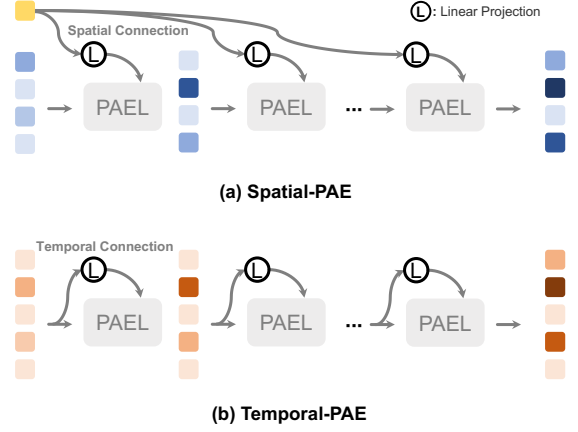


Fig. 4. Two different progressive attention encoders (PAE) for messaging: (a) Spatial-PAE and (b) Temporal-PAE.

Spatial-PAE models long-range dependency relationships on the filtered features activated by external information $\mathbf{F}_{ins} = [\mathbf{f}_{ins}, \mathbf{f}_{ins}, \dots, \mathbf{f}_{ins}] \in \mathbb{R}^{d \times r_k}$ as

$$\widehat{\mathbf{F}}_v^i = \text{PAEL}(\mathbf{F}_v^{i-1}, \mathbf{W}_s^i \mathbf{F}_{ins}), \quad i = 1, 2, \dots, n_v, \quad (11)$$

where $\widehat{\mathbf{F}}_v^i = [\widehat{\mathbf{f}}_{r_1}^i, \dots, \widehat{\mathbf{f}}_{r_k}^i]$ is the output of i -th PAEL, $\mathbf{F}_v^0 = \mathbf{F}_v$, $\widehat{\mathbf{f}}_{r_1}^i$, and $\mathbf{W}_s^i \in \mathbb{R}^{d \times d}$ denotes the i -th weights of linear projection. Then we can get an unbiased local correlated embedding $\mathbf{f}_{loc} \in \mathbb{R}^{d \times 1}$ as

$$\mathbf{f}_{loc} = \text{Head}(\widehat{\mathbf{f}}_{r_1}^{n_v}), \quad (12)$$

where $\text{Head}(\cdot)$ represents mapping the head embedding of the last layer to unbiased embedding. To preserve global semantic correlations, the final visual embedding is obtained as $\mathbf{v}_{emb} = \mathbf{f}_{cls} + \mathbf{f}_{loc}$.

Temporal-PAE (see Figure 4(b)) establishes a temporal connection to the input sequence of the previous time step via linear projection. In TEL, positional encoding may not effectively capture positional relationships within a sequence. Temporal-PAE computes the attention map using outputs from both the previous and current time steps, addressing the ambiguity and inaccuracies in position information that arise with deeper self-attention layers. This allows Temporal-PAE to recursively activate text features, which can be expressed as follows

$$\widehat{\mathbf{F}}_t^i = \text{PAEL}(\mathbf{F}_t^{i-1}, \mathbf{W}_t^i \mathbf{F}_t^{i-1}), \quad i = 1, 2, \dots, n_t, \quad (13)$$

where $\widehat{\mathbf{F}}_t^i = [\widehat{\mathbf{t}}_{cls}^i, \widehat{\mathbf{F}}_t^i]$ is the output of i -th PAEL, $\mathbf{F}_t^0 = [\mathbf{t}_{cls}, \mathbf{F}_t]$, $\mathbf{W}_t^i \in \mathbb{R}^{d \times d}$ denotes the i -th weights of linear projection, and $\widehat{\mathbf{F}}_t^i = [\widehat{\mathbf{e}}_1^i, \widehat{\mathbf{e}}_2^i, \dots, \widehat{\mathbf{e}}_n^i]$. Then we can get an unbiased local correlated embedding $\mathbf{t}_{loc} \in \mathbb{R}^{d \times 1}$ as

$$\mathbf{t}_{loc} = \text{Head}(\widehat{\mathbf{t}}_{cls}^{n_t}). \quad (14)$$

Similarly, we add the global correlated feature to get the final text embedding as $\mathbf{t}_{emb} = \mathbf{t}_{cls} + \mathbf{t}_{loc}$.

3) *PIR-ITR and PIR-CLIP*: According to the PIR learning idea, we first designed the soft belief strategy in inheritance of the previous hard belief [28] strategy of PIR-ITR. For PIR-ITR with soft belief strategy, we first obtain positive remote sensing image-text pairs $\{(I_{img}^1, T_{txt}^1, S_{cls}^1), (I_{img}^2, T_{txt}^2, S_{cls}^2), \dots, (I_{img}^m, T_{txt}^m, S_{cls}^m)\}$ from the remote sensing image-text datasets $\mathcal{D}_{img-txt}$. Then, the image I_{img} and text T_{txt} are encoded separately to obtain the corresponding visual features $[f_{cls}, F_v]$, instruction embeddings f_{ins} and textual features $[t_{cls}, F_t]$. After that, we compute the belief matrix \mathcal{M}_j^{bel} of visual features and instruction embeddings and calculate the rank R_j of element \mathcal{M}_j^{bel} in batch training. For each element F_i of dimension d in $[f_{cls}, F_v] \in \mathbb{R}^{d \times (m+1)}$, we get rank-weighted visual features F'_v . Finally, we can use Spatial-PAE and Temporal-PAE to get final v_{emb} and t_{emb} respectively.

The PIR-ITR directly performs the PIR learning paradigm after visual and text encoder processing for the above closed-domain retrieval. However, this complex and large structure is not easy to train on large-scale data. For PIR-CLIP, we first pre-train on RS5M dataset [17] using CLIP with contrastive loss, then fine-tune visual representation from RSITR datasets. The fine-tuning process is similar to PIR-ITR, with the key difference being that the visual backbone is updated using the base ViT and ResNet models, while the text encoder is replaced by a language transformer trained on a large-scale remote sensing corpus, eliminating the need for an additional Spatial-PAE. Unlike PIR-ITR, PIR-CLIP modifies the ViT structure by employing convolution for patching, followed by a soft belief strategy, and then a transformer encoder to facilitate interaction between visual and instructional features.

D. Loss Function

1) *Contrastive Loss*: In RSITR, triplet loss [7] is commonly used for model optimization. However, contrastive loss provides better optimization performance, as shown in the comparison between $VSE_2(TL)$ and $VSE_2(CL)$ in Table I. Therefore, we adopt contrastive loss [55] to optimize our model, as it requires only pairwise similarity calculations without the need for additional negative samples.

Given the v_{emb} and t_{emb} embedded by the PIR-ITR or PIR-CLIP from batch image-text pairs, we calculate the cosine similarity of them as $s_{i,j} = v_i^T t_j$. Then we can get the contrastive loss as

$$\mathcal{L}_c = -\frac{1}{N} \sum_{i=1}^N \left[\log \frac{\exp(s_{i,i}/\tau)}{\sum_{j=1}^N \exp(s_{i,j}/\tau)} + \log \frac{\exp(s_{i,i}/\tau)}{\sum_{j=1}^N \exp(s_{j,i}/\tau)} \right], \quad (15)$$

where τ is the temperature parameter.

2) *Affiliation Loss*: Most current retrieval tasks focus solely on pair-wise losses, such as contrastive loss [15], [56] and triplet loss [7], without fully accounting for the distributional characteristics of the data (see Figure 5(a)). To address this, we propose affiliation loss, which leverages the distributional characteristics of remote sensing data to minimize the distance

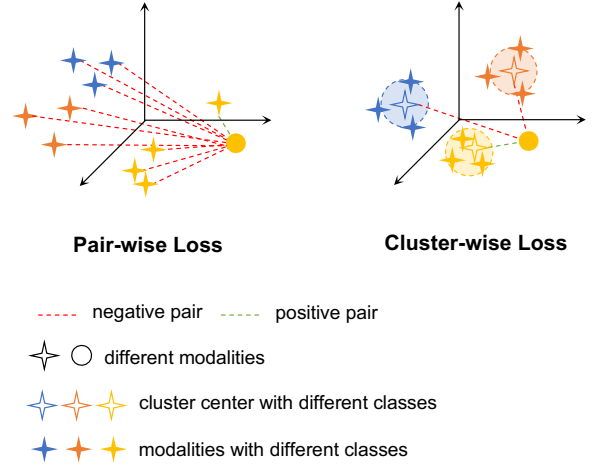


Fig. 5. Pair-wise loss and cluster-wise loss.

between each modality and the clustering center of its affiliated category [12], as illustrated in Figure 5(b).

Affiliation loss is a cluster-based loss [57] designed to reduce semantic confusion zones [12] by incorporating contrastive learning and scene category information. Figure 6 presents numpy-like pseudocode for the affiliation loss. Given a mini-batch sample, we can categorize them into C classes based on scene category information¹. For each image, its corresponding text is grouped into one category, so that we can get the positive pairs $\{(v_i, t_i^*) \mid i = 1, 2, \dots, N\}$, where t_i^* represents the clustering center corresponding to the i -th text. For each text, they are in a similar way as before. We can calculate the cosine similarity of vision-to-text $s_{i,j}^v = v_i^T t_j^*$ and the cosine similarity of text-to-vision $s_{j,i}^t = t_j^{*T} v_i$. Then we can obtain the attribution loss representations as

$$\mathcal{L}_a = -\frac{1}{N} \sum_{i=1}^N \left[\log \frac{\exp(s_{i,i}^v/\tau)}{\sum_{j=1}^N \exp(s_{i,j}^v/\tau)} + \log \frac{\exp(s_{i,i}^t/\tau)}{\sum_{j=1}^N \exp(s_{j,i}^t/\tau)} \right]. \quad (16)$$

and we can get the final loss function as

$$\mathcal{L}_{total} = \mathcal{L}_c + \lambda_{cs} \mathcal{L}_a, \quad (17)$$

where λ_{cs} is the center scale, indicating the extent of clustering at the category center.

V. EXPERIMENTS

A. Datasets

1) *RSICD Dataset*: RSICD contains 10,921 images with a resolution of 224×224 , each with five captions. We follow [11], [21] in dividing 7,862 training images, 1,966 validation images, and 1,093 test images.

2) *RSITMD Dataset*: RSITMD contains 4743 images with a resolution of 256×256 , each with five more fine-grained than RSICD. We follow [11] in 3,435 training images, 856 validation images, and 452 test images.

¹The RSICD and RSITMD datasets contain category information, which we can get from file name of images.

```

# I_e [n, d_e] - image embedding
# T_e [n, d_e] - text embedding
# cls [n, ] - the category of image
# t - learned temperature parameter

# category equality matrix [n, n]
cls_ = cls[:, np.newaxis]
cls_eq = np.equal(cls_, cls_.T)

# cluster center
I_centers_cls = []
T_centers_cls = []
for i in range(n):
    # mask different category [n, d_e]
    cls_eq_i = cls_eq[i][:, np.newaxis]
    cls_mask = np.tile(cls_eq_i, (1, I_e.shape[1]))
    # number of nonzero element
    n_nzero = np.sum(cls_eq_i, axis=0)
    # i-th image and text center of i
    I_center = np.sum(I_e * cls_mask, axis=0) / n_nzero
    T_center = np.sum(T_e * cls_mask, axis=0) / n_nzero
    I_centers_cls.append(I_center)
    T_centers_cls.append(T_center)
# image and text cluster centers by category [n, d_e]
I_centers_cls = np.concatenate(I_centers_cls, axis=0)
T_centers_cls = np.concatenate(T_centers_cls, axis=0)

# scaled pairwise cosine similarities [n, n]
logits_I2T = np.dot(I_e, T_centers_cls.T) * np.exp(t)
logits_T2I = np.dot(T_e, I_centers_cls.T) * np.exp(t)

# symmetric loss function
labels = np.arange(n)
loss_I2T = cross_entropy_loss(logits_I2T, labels)
loss_T2I = cross_entropy_loss(logits_T2I, labels)
loss = (loss_I2T + loss_T2I) / 2

```

Fig. 6. Numpy-like pseudocode of affiliation loss.

3) *RS5M Dataset*: RS5M [17] contains approximately 5 million remote sensing image-text pairs obtained by filtering publicly available remote sensing image-text datasets and captioning label-only remote sensing datasets with pre-trained image caption models. Our work uses the RS5M dataset as a pre-training dataset for PIR-CLIP.

B. Metrics

In accordance with previous RSITR studies [11], [12], [21], [39], we adopt the metrics of $R@K$ ($K = 1, 5, 10$) and mR to evaluate the effectiveness of our method. $R@K$ measures the percentage of correctly matched pairs within the top K retrieved results, while mR calculates the average of $R@K$ values, providing an overall assessment of the retrieval performance.

C. Implementation Details

For closed-domain retrieval, Swin Transformer is used as the vision encoder, pre-trained on ImageNet [58] using Swin-T (tiny version)², and BERT is used as the text encoder with pre-trained parameters from BERT-B (base version) provided by the official source³. The output dimensions for both vision and text encodings are set to 768 and then linearly mapped to 512 dimensions. Both self-attention and cross-attention have a head size of 8 and a dropout rate of 0.2, with different numbers of repeat units (2 for Spatial-PAE and 3 for Temporal-PAE).

ResNet-50 pre-trained on AID dataset [52] is used as the instruction encoder, with the second-to-last layer as an output of size 1024, linearly mapped to 512 dimensions. The contrastive and attribution losses have a temperature coefficient of 0.07 and a center factor of 1. For open-domain retrieval, ResNet-50 + ViT-B and Transformer are used as visual and textual backbones to align vanilla CLIP. We train a modified ResNet-50 on the AID dataset [52] and freeze the parameters before the attention pool layer during CLIP tuning. The pre-training epoch is set to 20, the batch size to 256, the fine-tuning is set to 10, and the batch size to 512, and the training samples go through 1,000,000 steps per epoch. Other settings are the same as for PIR-ITR. Model codes and checkpoints are open-sourced at <https://github.com/jaychempan/PIR-CLIP>.

D. Performance Comparisons

1) *State-of-the-art methods*: We compare and analyze the closed-domain and open-domain methods separately.

Closed-domain methods can be divided into three groups: *traditional image-text retrieval methods*, VSE_0 [43], SCAN [35], CAMP [39], and CAMERA [44], *remote sensing image-text retrieval methods*, LW-MCR [39], AMFMN [21], GaLR [11], KCR [10], SWAN [12], HVSA [59], and DOVE [54], and *Transformer-based backbone methods*, VSE_1 , VSE_2 [43] and $VSE_2 + TEL$. For SCAN, CAMP, and CAMERA, RoI Trans [61] with ResNet-50 as backbone⁴ pre-trained on DOTA [62] is used to detect significant objects. For *remote sensing image-text retrieval methods*, we pick the best results from the original paper to make the experiments as fair as possible since the experiments are difficult to be reproduced on RSICD and RSITMD. To be as fair as possible, we add *Transformer-based backbone methods*⁵ compared with PIR-ITR, a further improvement of the VSE method. VSE_i ($i = 0, 1, 2$) represents different vision and text backbones and TEL denotes the Transformer encoder layer. We also marked the corresponding loss function on the method (TL: triplet loss, CL: contrastive loss). “PIR-ITR with hard” and “PIR-ITR with soft” is PIR-ITR with hard and soft belief strategy.

Open-domain methods is to train a visual-semantic embedding model (VSE) with a dual-tower structure using natural language-supervised visual representations on large-scale image-text pairs dataset. CLIP [15], RemoteCLIP [16], GeoRSCLIP [17] and SkyCLIP [18] are respectively trained on WIT, RET-3 + DET-10 + SEG-4, RS5M and SkyScript, as shown in Table II. RET-3 is a combination of RSICD, RSITMD and UCM-Captions [63] datasets and follows the same method of de-duplication as RmoteCLIP [16] to avoid data leakage. We add RET-2 followed by GeoRSCLIP [17], a combination of RSICD and RSITMD that is also de-duplicated. We denote the official CLIP of 400 million image-text pairs from the Internet as WIT(CLIP). According to data availability, we pre-train our proposed PIR-CLIP on the RS5M dataset [17], which is the largest remote sensing image-text

⁴<https://github.com/open-mmlab/mrotate>

⁵In closed-domain methods, most of them use BERT for text feature extraction, different from open-domain methods that use vanilla Transformer for the purpose of establishing a foundation model.

²<https://github.com/microsoft/Swin-Transformer>

³<https://github.com/google-research/bert>

TABLE I
COMPARISON RETRIEVAL RESULTS OF THE CLOSED-DOMAIN IMAGE-TEXT RETRIEVAL ON RSICD AND RSITMD.

Method	Params	Backbone vision / text	RSICD Dataset			RSITMD Dataset		
			Image-query-Text R@1 / R@5 / R@10	Text-query-Image R@1 / R@5 / R@10	mR	Image-query-Text R@1 / R@5 / R@10	Text-query-Image R@1 / R@5 / R@10	mR
VSE_0 [43] (TL)	29 M	ResNet-50 / GRU	4.56 / 16.73 / 22.94	4.37 / 15.37 / 25.35	14.89	9.07 / 21.61 / 31.78	7.73 / 27.80 / 41.00	23.17
SCAN i2t [35]	60 M	RoI Trans / GRU	4.82 / 13.66 / 21.99	3.93 / 15.20 / 25.53	14.19	8.92 / 22.12 / 33.78	7.43 / 25.71 / 39.03	22.83
SCAN i2i [35]	60 M	RoI Trans / GRU	4.79 / 16.19 / 24.86	3.82 / 15.70 / 28.28	15.61	7.01 / 20.58 / 30.90	7.06 / 26.49 / 42.21	22.37
CAMP [39]	63 M	RoI Trans / GRU	4.64 / 14.61 / 24.09	4.25 / 15.82 / 27.82	15.20	8.11 / 23.67 / 34.07	6.24 / 26.37 / 42.37	23.47
CAMERA [44]	64 M	RoI Trans / BERT	4.57 / 13.08 / 21.77	4.00 / 15.93 / 26.97	14.39	8.33 / 21.83 / 33.11	7.52 / 26.19 / 40.72	22.95
LW-MCR [39]	-	CNNs / CNNs	3.29 / 12.52 / 19.93	4.66 / 17.51 / 30.02	14.66	10.18 / 28.98 / 39.82	7.79 / 30.18 / 49.78	27.79
AMFMN [21]	36 M	ResNet-18 / GRU	5.21 / 14.72 / 21.57	4.08 / 17.00 / 30.60	15.53	10.63 / 24.78 / 41.81	11.51 / 34.69 / 54.87	29.72
GalR [11]	46 M	ResNet-18+ppyolo / GRU	6.59 / 19.85 / 31.04	4.69 / 19.48 / 32.13	18.96	14.82 / 31.64 / 42.48	11.15 / 36.68 / 51.68	31.41
KCR [10]	-	ResNet-101 / BERT	5.95 / 18.59 / 29.58	5.40 / 22.44 / 37.36	19.89	-	-	-
SWAN [12]	40 M	ResNet-50 / GRU	7.41 / 20.13 / 30.86	5.56 / 22.26 / 37.41	20.61	13.35 / 32.15 / 46.90	11.24 / 40.40 / 60.60	34.11
HVSA [59]	-	ResNet-50 / GRU	7.47 / 20.62 / 32.11	5.51 / 21.13 / 34.13	20.61	13.20 / 32.08 / 45.58	11.43 / 39.20 / 57.45	33.16
DOVE [54]	38 M	ResNet-50+RoI Trans / GRU	8.66 / 22.35 / 34.95	6.04 / 23.95 / 40.35	22.72	16.81 / 36.80 / 49.93	12.20 / 49.93 / 66.50	37.73
VSE_1 (CL)	131 M	ViT-B / BERT	9.06 / 22.78 / 32.75	5.32 / 19.47 / 33.71	20.52	12.83 / 31.19 / 46.24	9.60 / 36.59 / 54.42	31.81
VSE_2 (TL)	137 M	Swin-T / BERT	7.96 / 21.68 / 34.31	6.44 / 22.09 / 37.49	21.66	17.70 / 36.28 / 48.67	13.58 / 41.24 / 59.29	36.13
VSE_2 (CL)	137 M	Swin-T / BERT	10.52 / 25.07 / 36.78	6.11 / 23.64 / 38.28	23.40	16.15 / 40.04 / 53.10	10.75 / 38.98 / 60.18	36.53
VSE_2+PAEL	161 M	Swin-T / BERT	10.43 / 25.89 / 37.15	6.02 / 23.42 / 38.30	23.53	17.48 / 36.95 / 50.44	11.81 / 41.99 / 61.77	36.74
PIR-ITR with hard	161 M	Swin-T+ResNet-50 / BERT	9.88 / 27.26 / 39.16	6.97 / 24.56 / 38.92	24.46	18.14 / 41.15 / 52.88	12.17 / 41.68 / 63.41	38.24
PIR-ITR with soft	161 M	Swin-T+ResNet-50 / BERT	10.89 / <u>26.17</u> / <u>37.79</u>	7.17 / 25.07 / 41.06	24.69	18.36 / 42.04 / 55.53	<u>13.36</u> / <u>44.47</u> / 61.73	39.25

TABLE II
COMPARISON RETRIEVAL RESULTS OF THE OPEN-DOMAIN IMAGE-TEXT RETRIEVAL ON RSICD AND RSITMD. † IS ZERO-SHOT CLIP AND ‡ IS FINE-TUNE CLIP.

Method	Params	Backbone vision / text	RSICD Dataset		Image-query-Text R@1 / R@5 / R@10	Text-query-Image R@1 / R@5 / R@10	mR
			Pre-training Dataset	Fine-tuning Dataset			
CLIP † [15]	151 M	ViT-B / Transformer	WIT (CLIP)	-	4.76 / 12.81 / 19.12	4.70 / 15.43 / 25.01	13.64
CLIP-FT ‡ [15]	151 M	ViT-B / Transformer	WIT (CLIP)	RSICD	15.55 / 30.56 / 41.99	14.68 / 33.63 / 42.71	29.85
PE-RSITR ‡ [60]	151 M	ViT-B / Transformer	WIT (CLIP)	RSICD	14.13 / 31.51 / 44.78	11.63 / 33.92 / 50.73	31.12
RemoteCLIP † [16]	151 M	ViT-B / Transformer	RET-3 + DET-10 + SEG-4	-	17.02 / 37.97 / 51.51	13.71 / 37.11 / 54.25	35.26
RemoteCLIP † [16]	428 M	ViT-L / Transformer	RET-3 + DET-10 + SEG-4	-	18.39 / 37.42 / 51.05	14.73 / 39.93 / 56.58	36.35
SkyCLIP † [18]	151 M	ViT-B / Transformer	Skyscript	-	6.59 / 16.10 / 26.53	7.14 / 22.34 / 34.29	18.83
SkyCLIP † [18]	428 M	ViT-L / Transformer	Skyscript	-	7.04 / 17.75 / 27.08	6.40 / 21.21 / 34.00	18.91
GeoRSCLIP † [17]	151 M	ViT-B / Transformer	RS5M	-	11.53 / 28.55 / 39.16	9.52 / 27.37 / 40.99	26.18
GeoRSCLIP-FT ‡ [17]	151 M	ViT-B / Transformer	RS5M	RSICD	22.14 / 40.53 / 51.78	15.26 / 40.46 / 57.79	38.00
GeoRSCLIP-FT ‡ [17]	151 M	ViT-B / Transformer	RS5M	RET-2	21.13 / 41.72 / 55.63	15.59 / 41.19 / 57.99	38.87
PIR-CLIP ‡	189 M	ResNet-50+ViT-B / Transformer	RS5M	RSICD	<u>26.62</u> / 40.71 / 50.32	21.35 / <u>43.59</u> / 54.27	39.48
PIR-CLIP ‡	189 M	ResNet-50+ViT-B / Transformer	RS5M	RET-2	25.62 / <u>43.18</u> / 53.06	19.91 / 42.74 / 55.15	39.95
PIR-CLIP ‡	189 M	ResNet-50+ViT-B / Transformer	RS5M	RET-3	27.63 / 45.38 / <u>55.26</u>	<u>21.10</u> / 44.87 / 56.12	41.73
RSITMD Dataset							
CLIP † [15]	151 M	ViT-B / Transformer	WIT (CLIP)	-	5.31 / 17.26 / 25.00	5.84 / 22.74 / 34.82	18.50
CLIP-FT ‡ [15]	151 M	ViT-B / Transformer	WIT (CLIP)	RSITMD	25.00 / 48.23 / 62.17	23.72 / 49.38 / 63.63	45.35
PE-RSITR ‡ [60]	151 M	ViT-B / Transformer	WIT (CLIP)	RSITMD	23.67 / 44.07 / 60.36	20.10 / 50.63 / 67.97	44.47
RemoteCLIP † [16]	151 M	ViT-B / Transformer	RET-3 + DET-10 + SEG-4	-	27.88 / 50.66 / 65.71	22.17 / 56.46 / 73.41	49.38
RemoteCLIP † [16]	428 M	ViT-L / Transformer	RET-3 + DET-10 + SEG-4	-	28.76 / 52.43 / 63.94	23.76 / 59.51 / 74.73	50.52
SkyCLIP † [18]	151 M	ViT-B / Transformer	Skyscript	-	10.18 / 25.44 / 35.62	10.88 / 33.27 / 49.82	27.54
SkyCLIP † [18]	428 M	ViT-L / Transformer	Skyscript	-	12.61 / 28.76 / 38.05	10.62 / 34.73 / 51.42	29.37
GeoRSCLIP † [17]	151 M	ViT-B / Transformer	RS5M	-	19.03 / 34.51 / 46.46	14.16 / 42.39 / 57.52	35.68
GeoRSCLIP-FT ‡ [17]	151 M	ViT-B / Transformer	RS5M	RSITMD	30.09 / 51.55 / 63.27	23.54 / <u>57.52</u> / 74.60	50.10
GeoRSCLIP-FT ‡ [17]	151 M	ViT-B / Transformer	RS5M	RET-2	32.30 / 53.32 / 67.92	25.04 / 57.88 / 74.38	51.81
PIR-CLIP ‡	189 M	ResNet-50+ViT-B / Transformer	RS5M	RSITMD	30.97 / 58.19 / 71.02	25.62 / 55.27 / 75.00	52.68
PIR-CLIP ‡	189 M	ResNet-50+ViT-B / Transformer	RS5M	RET-2	<u>44.25</u> / 65.71 / 75.22	<u>28.45</u> / 54.65 / 68.05	<u>56.05</u>
PIR-CLIP ‡	189 M	ResNet-50+ViT-B / Transformer	RS5M	RET-3	45.58 / <u>65.49</u> / <u>75.00</u>	30.13 / 55.44 / 68.54	56.70

pairs dataset to our knowledge. Except for CLIP and SkyCLIP, which are chosen to be obtained by testing based on official weights, the results of the other methods are obtained from the original papers.

2) *Quantitative comparison of Closed-domain methods:* The experiments of closed-domain methods focus on the comparison of retrieval performance in a single dataset training and testing, as shown in Table I.

Quantitative comparison on RSICD. As shown in Table I, the remote sensing image-text retrieval method could perform better than the traditional image-text retrieval method. For Transformer-based backbone methods, we can find that using Swin Transformer [64] to extract vision features is superior to

ViT [24]. Comparing VSE_2 (TL) and VSE_2 (CL), it is found that the method using contrastive loss is better than the method using triplet loss. It is observed that the retrieval performance differs significantly with different vision and text backbones, where Swin-T+BERT > ViT+BERT > ResNet-50+GRU. We can find that Transformer has a better representation in RSITR than CNN. We can find that mR can reach 23.53 when using a combination of VSE_2+TEL , but the improvement is insignificant compared to VSE_2 . Our proposed method can significantly improve the overall retrieval performance, with mR reaching 24.69, an improvement of 4.9% (24.69 vs 23.53).

Quantitative comparison on RSITMD. Compared with RSICD, RSITMD has a more fine-grained text description.

Therefore, the retrieval performance of RSITMD is significantly higher than RSICD’s. As shown in Table I, traditional image-text retrieval methods perform unsatisfactorily on RSITMD and RSICD. For the remote sensing image-text retrieval methods, SWAN based on the CNN and GRU feature extraction method makes mR reach 34.11. For Transformer-based feature extraction methods, $VSE_2 + TEL$ makes mR reach 36.74. Our proposed method results in a 4.0% improvement in mR (39.24 vs 37.73), with I2T $R@1$ and T2I $R@1$ reaching 18.36 and 13.36, respectively.

3) *Quantitative comparison of Open-domain methods*: The experiments of open-domain methods is fine-tuned on a small dataset after pre-training on an additional large-scale dataset, as shown in Table II.

Quantitative comparison on RSICD. A comparison of the zero-shot CLIP results reveals that the retrieval performance of pre-training on different large-scale datasets varies significantly, with RemoteCLIP reaching 36.35 on the RSICD dataset. From the results of the RemoteCLIP and SkyCLIP experiments, we found that their ViT-L version of CLIP can only get a limited improvement compared to the ViT-B version. The pre-trained CLIP model on the massive WIT (CLIP) dataset can improve the mR from 13.64 to 29.85 after fine-tuning the RSICD dataset. Further fine-tuning on the RSITR dataset can further improve the performance of the retrieval dataset; GeoRSCLIP, fine-tuned on RET-2, can get mR results 38.87. PIR-CLIP fine-tuned on RSICD, RET-2, and RET-3 allowed further mR enhancement of 1.5%, 2.7%, and 7.3%, respectively, compared to the state-of-the-art method (38.87). Among them, our method has the largest $R@1$ enhancement for I2T and T2I, reaching 27.63 and 21.35. The above experimental results show that our two-stage CLIP-based PIR-CLIP method is important in enhancing the performance of image retrieval and text retrieval $R@1$.

Quantitative comparison on RSITMD. On the RSITMD dataset, RemoteCLIP achieved 50.52 on mR by relying on zero-shot capability. The pre-trained CLIP model on the massive WIT (CLIP) dataset can improve the mR from 18.50 to 45.35 after fine-tuning the RSITMD dataset. Compared to RemoteCLIP (ViT-L), which incorporates RET-3 in its pre-training stage, our PIR-CLIP improves mR by 9.6% with smaller parameters. GeoRSCLIP allows mR to reach 51.81 by fine-tuning on RET-2. PIR-CLIP fine-tuned on RSITMD, RET-2, and RET-3 allowed further mR enhancement of 1.7%, 8.2%, and 9.4%, respectively, compared to the state-of-the-art method (51.81). Among them, our method has the largest $R@1$ enhancement for I2T and T2I, reaching 45.58 and 30.13. The above results show that our proposed PIR-CLIP can enhance visual representation and improve retrieval performance using the vision instruction fine-tuning approach.

4) *Visualization of results*: Figure 7 visualizes the top 5 retrieval results, including Image-query-Text (left) and Text-query-Image (right). In Image-query-Text, the blue box represents the query, the green text represents the mutual matching retrieval results, and the red one indicates the mismatched results; in Text-query-Image, the blue text represents the query, the green box represents the mutual matching retrieval results, and the red one indicates

the mismatched results. In Image-query-Text, most of the top 5 retrieval results are matching text for an image with only five matching texts. In Text-query-Image, matching images among the top 5 retrieval results rank first or second for a text with only one matching image. We find that PIR-CLIP will outperform PIR-ITR in image and text retrieval. However, in Text-query-Image results, the top 5 returned image retrieval results of PIR-ITR are more similar, and the retrieval results of PIR-CLIP have a higher rank, with the differences in the top 5 returned results being more significant. However, some retrieval results are also similar in semantics to distinguished, indicating that there is still room for further improvement.

E. Ablation Studies

In this section, we design twelve sets of experiments (the first eight is for PIR-ITR, else for PIR-CLIP) to demonstrate the effectiveness of the proposed three modules Spatial-PAE, Temporal-PAE and affiliation loss (\mathcal{L}_a), as shown in Table III. The *baseline* group represents the removal of the above three modules as the blank control group. *CLIP-baseline* is PIR-CLIP removes Spatial-PAE and attribution loss; other conditions remain the same.

1) *Effects of Vision Instruction Representation*: From the experimental results of +S-PAE, we find that using Spatial-PAE alone leads to a small increase in mR compared to the experimental results of *baseline*, with a significant increase in T2I $R@1$. From the experimental results of +S-PAE+T-PAE, we find that Spatial-PAE increases mR from 36.95 to 37.25 compared to the experimental results of +T-PAE, where Spatial-PAE increases more for I2T $R@10$ and T2I $R@10$. From the experimental results of +S-PAE+T-PAE+ \mathcal{L}_a , mR is improved by 2.6% compared to the experimental results of +T-PAE+ \mathcal{L}_a , where I2T $R@1$ increases from 17.04 to 18.14 and T2I $R@1$ increases from 11.81 to 12.17. For PIR-CLIP, we find that Spatial-PAE increases mR from 45.35 to 48.02 compared with the experimental results of +S-PAE \dagger and *CLIP-baseline*, and increases mR from 48.16 to 52.68 compared with the experimental results of + \mathcal{L}_a and +S-PAE \dagger + \mathcal{L}_a . With the above results, we find that Spatial-PAE can significantly improve vision representation and enhance the ability of Text-query-Image.

2) *Effects of Language Cycle Attention*: From the experimental results of +T-PAE, we find that Temporal-PAE can respectively improve 24.6% and 35.8% on I2T $R@1$ and T2I $R@1$ compared to the experimental results of *baseline*. From the experimental results of +S-PAE+T-PAE, we can observe that a 1.2% improvement in mR compared to the experimental results of +S-PAE. From the experimental results of +S-PAE+T-PAE+ \mathcal{L}_a , Temporal-PAE results in a 1.4% improvement in mR compared to the experimental results of +S-PAE+ \mathcal{L}_a , where I2T $R@1$ is improved from 16.81 to 18.14 and T2I $R@1$ is improved from 11.59 to 12.17. Comparing the experimental group +S-PAE with +S-PAE+T-PAE and the experimental group + \mathcal{L}_a with +T-PAE+ \mathcal{L}_a , we find that the effect of Temporal-PAE on the Image-query-Text and Text-query-Image task is positive. With the above results,

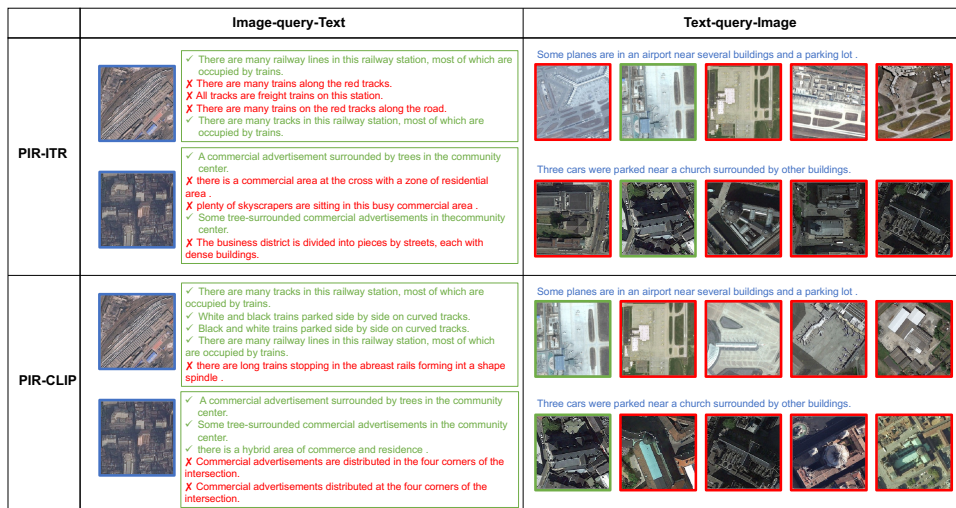


Fig. 7. The visualization of the top 5 retrieval results includes Image-query-Text (left) and Text-query-Image (right). Blue text and boxes represent queries, green text and boxes represent matching retrieval results, and red text and boxes indicate mismatched retrieval results.

TABLE III

RESULTS OF ABLATION EXPERIMENTS WITH DIFFERENT MODULES ON THE RSITMD TEST SET. UNLIKE THE SPATIAL-PAE OF PIR-ITR, THIS SPATIAL-PAE † OF PIR-CLIP IS BASED ON A MODIFIED ViT.

Method	Image-query-Text R@1 / R@5 / R@10	Text-query-Image R@1 / R@5 / R@10	mR
<i>baseline</i>	16.15 / 40.04 / 53.10	10.75 / 38.98 / 60.18	36.53
+S-PAE	16.59 / 38.50 / 54.65	12.88 / 40.04 / 58.19	36.81
+T-PAE	20.13 / 41.15 / 53.10	14.60 / 38.89 / 53.81	36.95
+ \mathcal{L}_a	<u>19.25</u> / 36.95 / 52.88	10.88 / 39.51 / 59.87	36.56
+S-PAE+T-PAE	17.04 / 39.16 / <u>54.42</u>	<u>13.50</u> / 40.04 / 59.34	37.25
+S-PAE+ \mathcal{L}_a	16.81 / 40.04 / 55.31	11.59 / 41.50 / 61.02	37.71
+T-PAE+ \mathcal{L}_a	17.04 / 38.72 / 53.76	11.81 / 41.64 / 60.58	37.26
+S-PAE+T-PAE+ \mathcal{L}_a	18.14 / 41.15 / 52.88	12.17 / 41.68 / 63.41	38.24
<i>CLIP-baseline</i>	25.00 / 48.23 / 62.17	23.72 / 49.38 / 63.63	45.35
+S-PAE †	24.56 / <u>53.32</u> / <u>66.37</u>	21.02 / 51.86 / <u>71.02</u>	48.02
+ \mathcal{L}_a	<u>27.65</u> / 52.21 / 63.94	25.49 / 53.10 / 66.59	48.16
+S-PAE † + \mathcal{L}_a	30.97 / 58.19 / 71.02	25.62 / 55.27 / 75.00	52.68

TABLE IV

RESULTS OF EXPERIMENTS OF FILTER SIZE IN SPATIAL-PAE ON THE RSITMD TEST SET.

PIR-ITR Filter Size	Image-query-Text R@1 / R@5 / R@10	Text-query-Image R@1 / R@5 / R@10	mR
$r_k=10$ with hard	17.26 / 40.71 / <u>54.65</u>	13.01 / 41.06 / 61.19	37.98
$r_k=20$ with hard	17.48 / 39.60 / 52.21	13.50 / 42.48 / <u>62.74</u>	38.00
$r_k=30$ with hard	19.03 / 37.83 / 49.78	12.83 / 41.90 / 62.08	37.24
$r_k=40$ with hard	18.14 / <u>41.15</u> / 52.88	12.17 / 41.68 / 63.41	38.24
$r_k=50$ with hard	18.36 / 37.61 / 50.88	13.10 / <u>42.88</u> / 62.04	37.48
$r_k=50$ with soft	<u>18.36</u> / 42.04 / 55.53	<u>13.36</u> / 44.47 / 61.73	39.25

we find that Temporal-PAE balances with vision representation to improve retrieval performance.

3) *Effects of Affiliation Loss*: From the experimental results of + \mathcal{L}_a , we find that \mathcal{L}_a alone can significantly improve I2T R@1 compared to the experimental results of *baseline*, which is improved from 16.15 to 19.25. From the experimental results of +S-PAE+T-PAE+ \mathcal{L}_a , it can be observed affiliation loss could improve mR by 2.7% compared to the experimental results of +S-PAE+T-PAE, where I2T R@1 is improved from 17.04 to 18.14. For PIR-CLIP, we find that \mathcal{L}_a increases mR

from 45.35 to 48.16 compared with the experimental results of + \mathcal{L}_a and *CLIP-baseline*, and increases mR from 48.02 to 52.68 compared with the experimental results of +S-PAE † and +S-PAE † + \mathcal{L}_a . From the above results, we can conclude that affiliation loss can significantly improve vision and text representations, which can help Spatial-PAE and Temporal-PAE to perform long-range dependency modeling.

F. Parameter Evaluation

1) *Filter Size in PIR*: For PIR-ITR with hard belief strategy, the visual features extracted based on Transformer contain much semantic noise, and some of the key features are more representative of the visual representation, so we use for unbiased correction of the visual representation. The maximum number of Vision Transformer output features is 50, and we control the number of key features by adjusting the filter size. Table IV shows the bidirectional retrieval results on the RSITMD with different filter sizes r_k (see Equation 4). We can find that when $r_k=10$, I2T R@10 is the largest, reaching 54.65; when $r_k=20$, mR reaches 38.00, and T2I R@1 is the largest, reaching 13.50; when $r_k=30$, I2T R@10 is the largest, but mR are relatively low compared to others; when $r_k=40$, mR is the largest, reaching 38.24, and the key feature is more representative of visual features at this time; when $r_k=50$, mR is 37.48 smaller than $r_k=10, 20, 40$ indicating that some key features are susceptible to deactivation by semantic noise. For PIR-ITR with soft belief strategy, it can further enhance the image retrieval and text retrieval performance with mR reaching up to 39.25. From the above experimental results, it can be concluded that semantic noise contained in remote-sensing images deactivates key features, and the retrieval performance can be effectively improved by reducing the dependence on partial features.

2) *Center Scale of Affiliation Loss*: The affiliation loss is used to reduce the semantic confusion region in the common subspace, and choosing an appropriate loss factor can improve the bidirectional retrieval performance. Since affiliation loss

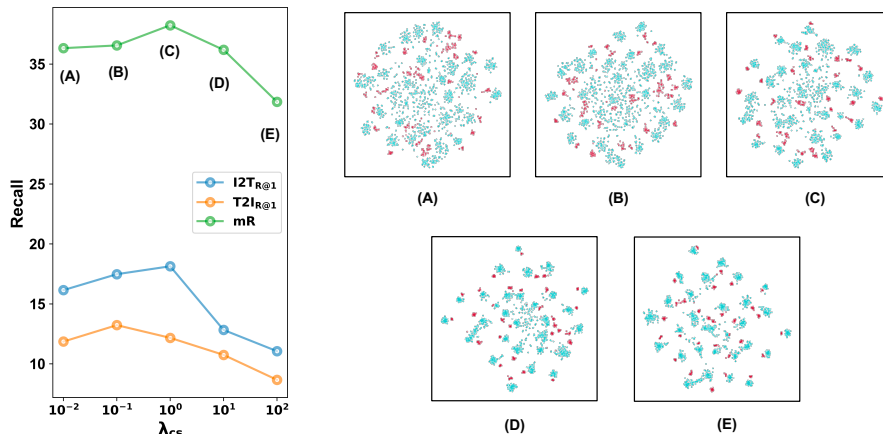


Fig. 8. The effect of the center scale on retrieval results (left) and RSITMD test set visualized with t-SNE [22] in the embedding space (right), the red squares represent vision embeddings, and the blue triangles represent text embeddings.

affects the degree of aggregation within a class, we also refer to this loss factor as the center scale, which measures the degree of aggregation within a class. The left side of Figure 8 shows the retrieval performance on the RSITMD at different center scales λ_{cs} , and the right side corresponds to the visualization of the embedding space at different center scales. As the center scale increases, the inter-class constraints are enhanced, and the semantic confusion zones are gradually reduced (A to E of Figure 8). However, the retrieval performance shows an increase followed by a decrease, indicating that a proper center scale ($\lambda_{cs} = 10^0$) can effectively improve the retrieval performance, and too strong inter-class constraints do not necessarily improve the retrieval performance.

TABLE V
RESULTS OF EXPERIMENTS OF DIFFERENT INSTRUCTION STRATEGY ON THE RSITMD TEST SET.

Instruction Encoder	Pre-trained Dataset	Image-query-Text			Text-query-Image			mR
		R@1 / R@5 / R@10	R@1 / R@5 / R@10	R@1 / R@5 / R@10	R@1 / R@5 / R@10			
VGG-16	AID	16.15 / 37.61 / 52.21	11.77 / 40.88 / 61.95	36.76				
VGG-19	AID	19.47 / 38.94 / 53.10	12.52 / 39.91 / 61.28	37.54				
ResNet-50	AID	18.14 / 41.15 / 52.88	12.17 / <u>41.68</u> / 63.41	<u>38.24</u>				
ResNet-101	AID	17.26 / 39.38 / 52.88	11.81 / 41.02 / 61.55	37.32				
ViT	AID	15.71 / 37.39 / 51.11	12.43 / 41.73 / 60.18	36.42				
Swin-T	AID	15.93 / 36.28 / <u>53.32</u>	12.65 / 41.68 / 60.84	36.78				
VGG-16	ImageNet	16.81 / 36.28 / 49.12	12.70 / 41.28 / 62.04	36.37				
ResNet-50	ImageNet	16.81 / 38.27 / 52.21	13.81 / 41.68 / 61.64	37.40				
Swin-T	ImageNet	15.71 / <u>40.93</u> / 52.65	<u>13.01</u> / 40.31 / 60.18	37.13				
VGG-16	RESISC45	16.81 / 38.27 / 50.66	11.50 / 40.58 / 60.31	36.36				
ResNet-50	RESISC45	17.70 / 39.82 / 53.98	12.92 / 42.96 / <u>62.30</u>	38.28				
Swin-T	RESISC45	15.93 / 37.61 / 52.21	12.08 / 41.06 / 61.37	36.71				

G. Instruction Strategy Analysis

To explore the impact of different instruction strategies on retrieval performance, we use different types of models as instruction encoders on PIR-ITR with hard belief strategy, where each model is pre-trained on the AID [52] dataset, RESISC45 dataset [65] and ImageNet [66] datasets for the classification task. These are divided into two categories, the CNN-based encoders, including VGG16 [67], VGG-19 [67], ResNet-50 [51], and ResNet-101 [51], and the Transformer-based encoders, including ViT [24] and Swin-T [64]. Table V shows the experimental results of the instruction encoders on the RSITMD dataset. The experimental results show that using ResNet-50 pre-trained on the AID dataset and RESISC45 dataset as the instruction encoder is more effective, performing the best at 38.24 and 38.28. We find no significant increase on retrieval performance by looking at the pre-trained ViT and Swin-T on the AID dataset as instruction encoders. By comparing VGG-16 and ResNet-50 pre-trained on ImageNet, we find that the pre-training based on remote sensing scene classification has a more obvious instructive role in guiding the vision representation. The above experimental results show that using prior knowledge based on remote sensing scene recognition can enhance vision representation and, thus, retrieval performance.

VI. CONCLUSION

This paper proposes the PIR framework, a new paradigm that leverages prior knowledge from the remote sensing data domain for adaptive learning of vision and text representations. We first propose the PIR-ITR for remote sensing image-text retrieval. Notably, Spatial-PAE and Temporal-PAE are applied to perform long-range dependency modelling to enhance key feature representation. In vision representation, we utilize prior knowledge from remote sensing scene recognition to instruct unbiased vision representation and reduce semantic noise's impact. In text representation, Temporal-PAE activates the current time step based on the previous time step to enhance semantic representation capability. Finally, a cluster-wise attribution loss is used as an inter-class constraint to reduce semantic confusion zones in the common subspace. Building on this foundation, we propose PIR-CLIP to address semantic noise in remote sensing vision-language representations and enhance open-domain retrieval performance further. Comprehensive experiments are designed to validate the superiority and effectiveness of our approach on two benchmark datasets, RSICD and RSITMD.

REFERENCES

- [1] H. Guo, X. Su, C. Wu, B. Du, and L. Zhang, "Saan: Similarity-aware attention flow network for change detection with vhr remote sensing images," *IEEE Transactions on Image Processing*, vol. 33, pp. 2599–2613, 2024.
- [2] M. Chi, A. Plaza, J. A. Benediktsson, Z. Sun, J. Shen, and Y. Zhu, "Big data for remote sensing: Challenges and opportunities," *Proceedings of the IEEE*, vol. 104, no. 11, pp. 2207–2219, 2016.
- [3] X. Lu, B. Wang, X. Zheng, and X. Li, "Exploring models and data for remote sensing image caption generation," *IEEE Transactions on Geoscience and Remote Sensing*, vol. 56, no. 4, pp. 2183–2195, 2017.
- [4] Q. Yang, M. Ye, Z. Cai, K. Su, and B. Du, "Composed image retrieval via cross relation network with hierarchical aggregation transformer," *IEEE Transactions on Image Processing*, vol. 32, pp. 4543–4554, 2023.
- [5] Y. LeCun, L. Bottou, Y. Bengio, and P. Haffner, "Gradient-based learning applied to document recognition," *Proceedings of the IEEE*, vol. 86, no. 11, pp. 2278–2324, 1998.
- [6] S. Hochreiter and J. Schmidhuber, "Long short-term memory," *Neural computation*, vol. 9, no. 8, pp. 1735–1780, 1997.
- [7] A. Karpathy and L. Fei-Fei, "Deep visual-semantic alignments for generating image descriptions," in *Proceedings of the IEEE conference on computer vision and pattern recognition*, 2015, pp. 3128–3137.
- [8] T. Abdullah, Y. Bazi, M. M. Al Rahhal, M. L. Mekhalif, L. Rangarajan, and M. Zuair, "Textrs: Deep bidirectional triplet network for matching text to remote sensing images," *Remote Sensing*, vol. 12, no. 3, p. 405, 2020.
- [9] Y. Lv, W. Xiong, X. Zhang, and Y. Cui, "Fusion-based correlation learning model for cross-modal remote sensing image retrieval," *IEEE Geoscience and Remote Sensing Letters*, vol. 19, pp. 1–5, 2021.
- [10] L. Mi, S. Li, C. Chappuis, and D. Tuia, "Knowledge-aware cross-modal text-image retrieval for remote sensing images," in *Proceedings of the Second Workshop on Complex Data Challenges in Earth Observation (CDCEO 2022)*, 2022.
- [11] Z. Yuan, W. Zhang, C. Tian, X. Rong, Z. Zhang, H. Wang, K. Fu, and X. Sun, "Remote sensing cross-modal text-image retrieval based on global and local information," *IEEE Transactions on Geoscience and Remote Sensing*, vol. 60, pp. 1–16, 2022.
- [12] J. Pan, Q. Ma, and C. Bai, "Reducing semantic confusion: Scene-aware aggregation network for remote sensing cross-modal retrieval," in *Proceedings of the 2023 ACM International Conference on Multimedia Retrieval*, 2023, pp. 398–406.
- [13] A. B. Dieng, C. Wang, J. Gao, and J. Paisley, "Topicrnn: A recurrent neural network with long-range semantic dependency," *arXiv preprint arXiv:1611.01702*, 2016.
- [14] Y. Cao, J. Xu, S. Lin, F. Wei, and H. Hu, "Gcnet: Non-local networks meet squeeze-excitation networks and beyond," in *Proceedings of the IEEE/CVF international conference on computer vision workshops*, 2019, pp. 0–0.
- [15] A. Radford, J. W. Kim, C. Hallacy, A. Ramesh, G. Goh, S. Agarwal, G. Sastry, A. Askell, P. Mishkin, J. Clark *et al.*, "Learning transferable visual models from natural language supervision," in *International conference on machine learning*. PMLR, 2021, pp. 8748–8763.
- [16] F. Liu, D. Chen, Z. Guan, X. Zhou, J. Zhu, Q. Ye, L. Fu, and J. Zhou, "Remoteclip: A vision language foundation model for remote sensing," *IEEE Transactions on Geoscience and Remote Sensing*, vol. 62, pp. 1–16, 2024. [Online]. Available: <https://doi.org/10.1109/TGRS.2024.3390838>
- [17] Z. Zhang, T. Zhao, Y. Guo, and J. Yin, "Rs5m and georsclip: A large scale vision-language dataset and a large vision-language model for remote sensing," *IEEE Transactions on Geoscience and Remote Sensing*, pp. 1–1, 2024.
- [18] Z. Wang, R. Prabha, T. Huang, J. Wu, and R. Rajagopal, "Skyscript: A large and semantically diverse vision-language dataset for remote sensing," *Proceedings of the AAAI Conference on Artificial Intelligence*, vol. 38, pp. 5805–5813, Mar. 2024. [Online]. Available: <https://ojs.aaai.org/index.php/AAAI/article/view/28393>
- [19] T.-Y. Lin, M. Maire, S. Belongie, J. Hays, P. Perona, D. Ramanan, P. Dollár, and C. L. Zitnick, "Microsoft coco: Common objects in context," in *Computer Vision—ECCV 2014: 13th European Conference, Zurich, Switzerland, September 6–12, 2014, Proceedings, Part V 13*. Springer, 2014, pp. 740–755.
- [20] B. A. Plummer, L. Wang, C. M. Cervantes, J. C. Caicedo, J. Hockenmaier, and S. Lazebnik, "Flickr30k entities: Collecting region-to-phrase correspondences for richer image-to-sentence models," in *Proceedings of the IEEE international conference on computer vision*, 2015, pp. 2641–2649.
- [21] Z. Yuan, W. Zhang, K. Fu, X. Li, C. Deng, H. Wang, and X. Sun, "Exploring a fine-grained multiscale method for cross-modal remote sensing image retrieval," *arXiv preprint arXiv:2204.09868*, 2022.
- [22] L. Van der Maaten and G. Hinton, "Visualizing data using t-sne." *Journal of machine learning research*, vol. 9, no. 11, 2008.
- [23] J. Liang, J. Cao, G. Sun, K. Zhang, L. Van Gool, and R. Timofte, "Swinir: Image restoration using swin transformer," in *Proceedings of the IEEE/CVF international conference on computer vision*, 2021, pp. 1833–1844.
- [24] A. Dosovitskiy, L. Beyer, A. Kolesnikov, D. Weissenborn, X. Zhai, T. Unterthiner, M. Dehghani, M. Minderer, G. Heigold, S. Gelly *et al.*, "An image is worth 16x16 words: Transformers for image recognition at scale," *arXiv preprint arXiv:2010.11929*, 2020.
- [25] J. Devlin, M.-W. Chang, K. Lee, and K. Toutanova, "Bert: Pre-training of deep bidirectional transformers for language understanding," *arXiv preprint arXiv:1810.04805*, 2018.
- [26] H. Zhang, Y. Sun, Y. Liao, S. Xu, R. Yang, S. Wang, B. Hou, and L. Jiao, "A transformer-based cross-modal image-text retrieval method using feature decoupling and reconstruction," in *IGARSS 2022-2022 IEEE International Geoscience and Remote Sensing Symposium*. IEEE, 2022, pp. 1796–1799.
- [27] Q. Zou, L. Ni, T. Zhang, and Q. Wang, "Deep learning based feature selection for remote sensing scene classification," *IEEE Geoscience and Remote Sensing Letters*, vol. 12, no. 11, pp. 2321–2325, 2015.
- [28] J. Pan, Q. Ma, and C. Bai, "A prior instruction representation framework for remote sensing image-text retrieval," in *Proceedings of the 31st ACM International Conference on Multimedia*, 2023, pp. 611–620.
- [29] G. Mao, Y. Yuan, and L. Xiaoqiang, "Deep cross-modal retrieval for remote sensing image and audio," in *2018 10th IAPR Workshop on Pattern Recognition in Remote Sensing (PRRS)*. IEEE, 2018, pp. 1–7.
- [30] Z. Yuan, W. Zhang, C. Tian, Y. Mao, R. Zhou, H. Wang, K. Fu, and X. Sun, "Mcrn: A multi-source cross-modal retrieval network for remote sensing," *International Journal of Applied Earth Observation and Geoinformation*, vol. 115, p. 103071, 2022.
- [31] Q. Cheng, Y. Zhou, P. Fu, Y. Xu, and L. Zhang, "A deep semantic alignment network for the cross-modal image-text retrieval in remote sensing," *IEEE Journal of Selected Topics in Applied Earth Observations and Remote Sensing*, vol. 14, pp. 4284–4297, 2021.
- [32] L. Djoufack Basso, "Clip-rs: A cross-modal remote sensing image retrieval based on clip, a northern virginia case study," Ph.D. dissertation, Virginia Tech, 2022.
- [33] A. Vaswani, N. Shazeer, N. Parmar, J. Uszkoreit, L. Jones, A. N. Gomez, Ł. Kaiser, and I. Polosukhin, "Attention is all you need," *Advances in neural information processing systems*, vol. 30, 2017.
- [34] M. Gheini, X. Ren, and J. May, "On the strengths of cross-attention in pretrained transformers for machine translation," *arXiv preprint arXiv:2104.08771*, 2021.
- [35] K.-H. Lee, X. Chen, G. Hua, H. Hu, and X. He, "Stacked cross attention for image-text matching," in *Proceedings of the European conference on computer vision (ECCV)*, 2018, pp. 201–216.
- [36] H. Diao, Y. Zhang, W. Liu, X. Ruan, and H. Lu, "Plug-and-play regulators for image-text matching," *IEEE Transactions on Image Processing*, vol. 32, pp. 2322–2334, 2023.
- [37] X. Wei, T. Zhang, Y. Li, Y. Zhang, and F. Wu, "Multi-modality cross attention network for image and sentence matching," in *Proceedings of the IEEE/CVF conference on computer vision and pattern recognition*, 2020, pp. 10941–10950.
- [38] X. Xu, T. Wang, Y. Yang, L. Zuo, F. Shen, and H. T. Shen, "Cross-modal attention with semantic consistence for image-text matching," *IEEE transactions on neural networks and learning systems*, vol. 31, no. 12, pp. 5412–5425, 2020.
- [39] Z. Yuan, W. Zhang, X. Rong, X. Li, J. Chen, H. Wang, K. Fu, and X. Sun, "A lightweight multi-scale crossmodal text-image retrieval method in remote sensing," *IEEE Transactions on Geoscience and Remote Sensing*, vol. 60, pp. 1–19, 2021.
- [40] C. Bai, L. Huang, X. Pan, J. Zheng, and S. Chen, "Optimization of deep convolutional neural network for large scale image retrieval," *Neurocomputing*, vol. 303, pp. 60–67, 2018.
- [41] X. Zhang, C. Bai, and K. Kpalma, "Omcbir: Offline mobile content-based image retrieval with lightweight cnn optimization," *Displays*, vol. 76, p. 102355, 2023.
- [42] J. Chung, C. Gulcehre, K. Cho, and Y. Bengio, "Empirical evaluation of gated recurrent neural networks on sequence modeling," *arXiv preprint arXiv:1412.3555*, 2014.
- [43] F. Faghri, D. J. Fleet, J. R. Kiros, and S. Fidler, "Vse++: Improving visual-semantic embeddings with hard negatives," *arXiv preprint arXiv:1707.05612*, 2017.

- [44] L. Qu, M. Liu, D. Cao, L. Nie, and Q. Tian, "Context-aware multi-view summarization network for image-text matching," in *Proceedings of the 28th ACM International Conference on Multimedia*, 2020, pp. 1047–1055.
- [45] C. Li, W. Xu, S. Li, and S. Gao, "Guiding generation for abstractive text summarization based on key information guide network," in *Proceedings of the 2018 Conference of the North American Chapter of the Association for Computational Linguistics: Human Language Technologies, Volume 2 (Short Papers)*, 2018, pp. 55–60.
- [46] S. Dathathri, A. Madotto, J. Lan, J. Hung, E. Frank, P. Molino, J. Yosinski, and R. Liu, "Plug and play language models: A simple approach to controlled text generation," *arXiv preprint arXiv:1912.02164*, 2019.
- [47] A. Kirillov, E. Mintun, N. Ravi, H. Mao, C. Rolland, L. Gustafson, T. Xiao, S. Whitehead, A. C. Berg, W.-Y. Lo *et al.*, "Segment anything," *arXiv preprint arXiv:2304.02643*, 2023.
- [48] J. Yang, M. Gao, Z. Li, S. Gao, F. Wang, and F. Zheng, "Track anything: Segment anything meets videos," *arXiv preprint arXiv:2304.11968*, 2023.
- [49] T. Wang, J. Zhang, J. Fei, Y. Ge, H. Zheng, Y. Tang, Z. Li, M. Gao, S. Zhao, Y. Shan *et al.*, "Caption anything: Interactive image description with diverse multimodal controls," *arXiv preprint arXiv:2305.02677*, 2023.
- [50] C. Liu, Y. Zhang, H. Wang, W. Chen, F. Wang, Y. Huang, Y.-D. Shen, and L. Wang, "Efficient token-guided image-text retrieval with consistent multimodal contrastive training," *IEEE Transactions on Image Processing*, vol. 32, pp. 3622–3633, 2023.
- [51] K. He, X. Zhang, S. Ren, and J. Sun, "Deep residual learning for image recognition," in *Proceedings of the IEEE conference on computer vision and pattern recognition*, 2016, pp. 770–778.
- [52] G.-S. Xia, J. Hu, F. Hu, B. Shi, X. Bai, Y. Zhong, L. Zhang, and X. Lu, "Aid: A benchmark data set for performance evaluation of aerial scene classification," *IEEE Transactions on Geoscience and Remote Sensing*, vol. 55, no. 7, pp. 3965–3981, 2017.
- [53] A. Jaegle, S. Borgeaud, J.-B. Alayrac, C. Doersch, C. Ionescu, D. Ding, S. Koppula, D. Zoran, A. Brock, E. Shelhamer *et al.*, "Perceiver io: A general architecture for structured inputs & outputs," *arXiv preprint arXiv:2107.14795*, 2021.
- [54] Q. Ma, J. Pan, J. Chen, and C. Bai, "Direction-oriented visual-semantic embedding model for remote sensing image-text retrieval," *arXiv preprint arXiv:2310.08276*, 2023.
- [55] R. Hadsell, S. Chopra, and Y. LeCun, "Dimensionality reduction by learning an invariant mapping," in *2006 IEEE Computer Society Conference on Computer Vision and Pattern Recognition (CVPR'06)*, vol. 2. IEEE, 2006, pp. 1735–1742.
- [56] Y. Zeng, X. Zhang, and H. Li, "Multi-grained vision language pre-training: Aligning texts with visual concepts," *arXiv preprint arXiv:2111.08276*, 2021.
- [57] G. Li, B. Choi, J. Xu, S. S. Bhowmick, K.-P. Chun, and G. L.-H. Wong, "Shapenet: A shapelet-neural network approach for multivariate time series classification," in *Proceedings of the AAAI Conference on Artificial Intelligence*, vol. 35, no. 9, 2021, pp. 8375–8383.
- [58] A. Krizhevsky, I. Sutskever, and G. E. Hinton, "Imagenet classification with deep convolutional neural networks," *Communications of the ACM*, vol. 60, no. 6, pp. 84–90, 2017.
- [59] W. Zhang, J. Li, S. Li, J. Chen, W. Zhang, X. Gao, and X. Sun, "Hypersphere-based remote sensing cross-modal text-image retrieval via curriculum learning," *IEEE Transactions on Geoscience and Remote Sensing*, 2023.
- [60] Y. Yuan, Y. Zhan, and Z. Xiong, "Parameter-efficient transfer learning for remote sensing image-text retrieval," *IEEE Transactions on Geoscience and Remote Sensing*, 2023.
- [61] J. Ding, N. Xue, Y. Long, G.-S. Xia, and Q. Lu, "Learning roi transformer for oriented object detection in aerial images," in *Proceedings of the IEEE/CVF Conference on Computer Vision and Pattern Recognition*, 2019, pp. 2849–2858.
- [62] G.-S. Xia, X. Bai, J. Ding, Z. Zhu, S. Belongie, J. Luo, M. Datcu, M. Pelillo, and L. Zhang, "Dota: A large-scale dataset for object detection in aerial images," in *Proceedings of the IEEE conference on computer vision and pattern recognition*, 2018, pp. 3974–3983.
- [63] Y. Yang and S. Newsam, "Bag-of-visual-words and spatial extensions for land-use classification," in *Proceedings of the 18th SIGSPATIAL International Conference on Advances in Geographic Information Systems*, ser. GIS '10. New York, NY, USA: Association for Computing Machinery, 2010, p. 270–279.
- [64] Z. Liu, Y. Lin, Y. Cao, H. Hu, Y. Wei, Z. Zhang, S. Lin, and B. Guo, "Swin transformer: Hierarchical vision transformer using shifted windows," in *Proceedings of the IEEE/CVF international conference on computer vision*, 2021, pp. 10012–10022.
- [65] G. Cheng, J. Han, and X. Lu, "Remote sensing image scene classification: Benchmark and state of the art," *Proceedings of the IEEE*, vol. 105, no. 10, pp. 1865–1883, 2017.
- [66] J. Deng, W. Dong, R. Socher, L.-J. Li, K. Li, and L. Fei-Fei, "Imagenet: A large-scale hierarchical image database," in *2009 IEEE conference on computer vision and pattern recognition*. Ieee, 2009, pp. 248–255.
- [67] K. Simonyan and A. Zisserman, "Very deep convolutional networks for large-scale image recognition," *arXiv preprint arXiv:1409.1556*, 2014.